Geophysical Research Letters

RESEARCH LETTER
10.1029/2019GL082352

Short- and Long-Term Variations in the Reykjanes Geothermal Reservoir From Seismic Noise Interferometry

Pilar Sánchez-Pastor[1,2], Anne Obermann[3], Martin Schimmel[1], Cornelis Weemstra[4,5], Arie Verdel[6], and Philippe Jousset[7]

[1]Institute of Earth Sciences Jaume Almera, CSIC, Barcelona, Spain, [2]Departament de Dinàmica de la Terra i de l'Oceà, Universitat de Barcelona, Barcelona, Spain, [3]Swiss Seismological Service, ETH Zurich, Zurich, Switzerland, [4]Department of Geoscience and Engineering, Delft University of Technology, Delft, The Netherlands, [5]Royal Netherlands Meteorological Institute, De Bilt, The Netherlands, [6]Netherlands Organisation for Applied Scientific Research TNO, Utrecht, The Netherlands, [7]GFZ German Research Centre for Geosciences, Potsdam, Germany

Key Points:
- Identification of three elastic properties changes in time-frequency associated with abrupt injection and production rate variations
- Water deficit in the reservoir leads to a gradual seismic velocity decrease
- Seasonal production rate variations within the geothermal reservoir are observed as structural property changes

Supporting Information:
- Supporting Information S1

Correspondence to:
P. Sánchez-Pastor,
psanchezsp@gmail.com

Citation:
Sánchez-Pastor, P., Obermann, A., Schimmel, M., Weemstra, C., Verdel, A., & Jousset, P. (2019). Short- and long-term variations in the Reykjanes geothermal reservoir from seismic noise interferometry. *Geophysical Research Letters*, *46*. https://doi.org/10.1029/2019GL082352

Received 4 FEB 2019
Accepted 1 MAY 2019
Accepted article online 9 MAY 2019

Abstract The Reykjanes Geothermal System (RGS) is a high-temperature geothermal system located on the Reykjanes peninsula, a transtensional plate-boundary zone located on the southwestern tip of Iceland. The area is characterized by high seismicity, recent volcanism, and high-temperature geothermal fields. We use seismic noise records from April 2014 to August 2015 to study stress changes and potential deformation of the subsurface caused by injection and production operations at RGS through seismic interferometry. We retrieve continuous time series of waveform similarity values and seismic velocity changes during this period. The S-transform of the similarity values allows us to clearly identify three variations in the mechanical properties of the Reykjanes peninsula related to rapid changes of RGS production. In addition, we observe a slow seismic velocity decrease of 0.36%/year in the reservoir due to the water deficit and seasonal variations associated with the energy production demand.

Plain Language Summary The Mid-Atlantic Spreading Ridge divides the Reykjanes peninsula into two tectonic plates and causes the high volcanic activity that characterizes the area. The Reykjanes Geothermal System is one of the five high-temperature geothermal systems exploited in this peninsula. The energy production of Reykjanes Geothermal System has been increasing, causing drastic changes in reservoir conditions, such as, a man-made subsidence of around 10 cm in the area. We employ three current methodologies to monitor changes of mechanical and structural properties in the subsurface, using 1.5 years of continuous seismic records. We identify and locate three short-term variations associated with abrupt injection and production rate changes in Reykjanes Geothermal System. In addition, we observe a slow seismic velocity decrease due to the long-term water extraction, as well as variations associated with demand-driven seasonal fluctuations in the extraction rates.

1. Introduction

Despite the fact that early foundations have been laid in the 50s and 60s by seismologists such as Aki (1957) and Claerbout (1968), seismic interferometry (SI) gained most of its popularity over the last decade. SI refers to the principle of generating virtual source responses by cross-correlating existing seismic records (Bakulin & Calvert, 2006). Many applications have arisen that exploit the technique to infer characteristics of the subsurface (e.g., Draganov et al., 2007; Sens-Schönfelder & Wegler, 2011; Shapiro et al., 2005), the Sun (Duvall et al., 1993), the oceans (Roux & Fink, 2003; Woolfe et al., 2015), buildings (Kohler et al., 2007; Snieder & Safak, 2006), and the atmosphere (Fricke et al., 2014; Haney, 2009).

An important application of SI involves the monitoring of tiny changes of elastic and structural properties in a medium that can be picked up as waveform dilatations or distortions in the so called "coda," later-arriving multiply scattered waves (e.g., Beroza et al., 1995; Sens-Schönfelder & Wegler, 2006). The coda waves sample the medium very densely and are more sensitive to mechanical and structural changes than the direct arrivals. The technique is often referred to as coda wave interferometry (Snieder et al., 2002).

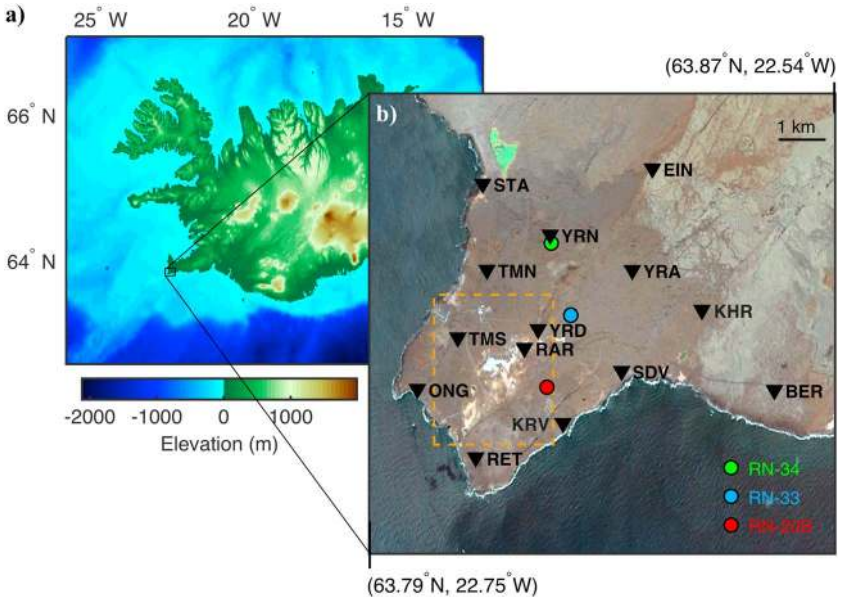

Figure 1. (a) Location and elevation map of Iceland. The black box marks the Reykjanes peninsula. (b) Map of the tip of the Reykjanes peninsula. The black triangles indicate the seismic stations used in this study. The circles show the location of three injection wells: RN-20B (red), RN-33 (blue), and RN-34 (green). The approximate location of the production area of the Reykjanes Geothermal System (RGS) is represented by the dashed orange square.

The ever-present ambient vibrations enable a continuous retrieval of virtual source responses and therefore remove the need for expensive and disturbing repetitive controlled sources. The continuous nature of the virtual source responses also implies that these do not suffer from a lack of repeatability, in contrast to the responses obtained from natural sources, such as earthquakes (e.g., Poupinet et al., 1984). The main condition required for monitoring is that the ambient vibrations are statistically robust over certain time windows. This permits repeatable virtual source responses, which then allow for structural changes to be studied. Due to this characteristic, the condition that the medium is illuminated uniformly from all angles, which is a requirement for accurate Green's function retrieval (Tsai, 2009; Weaver et al., 2009), can be relaxed for monitoring purposes (Hadziioannou et al., 2009).

Seismic monitoring using coda wave interferometry has been applied successfully on various scales (e.g., Obermann et al., 2014; Stähler et al., 2011) and in a variety of environments (Sens-Schönfelder & Wegler, 2011). Recently, the use of SI in a geothermal context has received considerable attention. In 2017, the cumulative global geothermal capacity reached over 14 GW; this figure is expected to rise to over 17 GW by 2023 (International Energy Agency (IEA), 2018; Hirschberg et al., 2015). Geothermal systems can be divided into "hydrothermal systems," which exploit existent and naturally profitable aquifers, and "enhanced geothermal systems," which enhance the permeability of the crystalline basement through high-pressure injection of fluids. To our knowledge, SI has only been used to probe enhanced geothermal systems (Hillers et al., 2015; Lehujeur et al., 2015; Obermann et al., 2015).

The RGS is a hydrothermal system located on the southwestern tip of the Reykjanes peninsula, where the Mid-Atlantic ridge comes ashore. This system has been exploited on a small scale for decades, but in 2006, a new power plant was installed. The associated increased production rate has caused drastic changes in reservoir conditions, for instance, a considerable drop of the pressure in the reservoir (Axelsson et al., 2015) and a subsidence of around 10 cm in the area (Keiding et al., 2010).

In this study, we assess the capability of SI to detect tiny mechanical and structural changes in RGS using ambient-seismic noise recorded by thirteen stations from April 2014 till August 2015 (Figure 1). During this period, the geothermal activity of the power plant was uninterrupted in different points of the peninsula. The lack of seismic records during a "calm period" causes a strong variability of the seismic medium response. Thus, we focus on the waveform similarity evolution (D'Hour et al., 2015; SÁnchez-Pastor et al., 2018) and time-lapse changes in velocity (e.g., Brenguier et al., 2011; Hadziioannou et al., 2009; Obermann

et al., 2014) using different methods to ascertain the robustness of our findings. We propose a new procedure to discriminate potential changes in time and frequency of such evolution curves through the computation of the S transform (Stockwell et al., 1996).

2. Geothermal Well Operations

The Mid-Atlantic Spreading Ridge divides the Reykjanes peninsula into two tectonic plates that part at an average of 2 cm/year. The transtensional plate boundary causes significant seismic and volcanic activity with NE-SW striking faults and fissures characterizing the area. The active volcanic systems derive their energy from cooling magma bodies in the crust, such as magma chambers, dykes, and other intrusions (Flóvenz et al., 2015; Gudmundsson, 1995; Gudmundsson & Thórhallsson, 1986). These important heat sources reach the surface and have been exploited since the settlement of Iceland in the ninth century. Nowadays, the utilization of the geothermal sources plays a fundamental role in the energy economy of Iceland (Ragnarsson, 2013).

On Reykjanes peninsula, five high-temperature geothermal systems are exploited; RGS is one of them. The development of this system started in 1956 with a single shallow well (~160 m). RGS expanded through the development of 14 deep production wells (around 2-km depth) and the construction of a geothermal plant of 100 MW in 2006 (Axelsson et al., 2015). In order to counteract the pressure drop in the reservoir and reduce the environmental effects of surface disposal, in 2009, the reinjection of sea water into the system began (Flóvenz et al., 2015). During the time period evaluated in this study, only one injection well was operating at 1.2 km of depth (RN-20B) and two were running for tracer tests (RN-33 and RN-34) at around 2-km depth (Figure 1). The extracted water volume is shown in Figure 2a together with the injected water volume of the three injection wells. The seismicity of the area does not show a direct correlation with the observed injection/production changes (supporting information Figure S4).

3. Data and SI

3.1. Seismic Network

We use 13 stations from the Reykjanes seismic array (Blanck et al., 2016; Weemstra et al., 2016) most of which were deployed in the context of the European Community's project IMAGE (Integrated Methods for Advanced Geothermal Exploration) from the beginning of April 2014 until August 2015 at the tip of the Reykjanes peninsula (Figure 1). The selected stations (Figure 1b) have been recording quasi-continuously for the 1.5 years of observation period at 100 samples per second. In the supporting information (Figure S1), we show the exemplary power spectrum density plots for the different types of sensors.

3.2. Computation of Autocorrelation and Cross Correlation

We compute autocorrelation and cross correlation using the vertical component of all seismic stations. For the computation of the correlations, we use the classical correlation approach (CC, Bensen et al., 2007) and the phase cross correlation approach (PCC; Schimmel, 1999). One-bit amplitude normalization and spectral whitening are commonly used as preprocessing for the classical approach to reduce its amplitude bias caused by seismicity and other energetic signals (Bensen et al., 2007). Here we compute geometrically normalized CCs, with (CCN) and without (CCG) such preprocessing. It is useful to note that the PCC is not affected by large amplitudes and does not require any preprocessing that could yield a loss of information in terms of waveform distortion (Schimmel et al., 2011, 2018). PCC has been successfully employed in other noise-based monitoring and imaging studies (e.g., D'Hour et al., 2015; Romero & Schimmel, 2018; SÁnchez-Pastor et al., 2018).

Restricting the frequency band of the correlations, the convergence of the virtual source response improves significantly (Roux et al., 2005). We therefore compare the waveform convergence of the three above-mentioned approaches (CCN, CCG, and PCC) in three different frequency bands (0.1–1.0, 0.5–2.0, and 2.0–5.0 Hz). This comparison is made separately for different interstation distances (supporting information Figure S2). Since most of the changes in injection and production rate in the RGS happen over a very short period of time, fast convergence of the stabilization of the correlations is important. Irrespective of the method, the shorter the interstation distance and/or the lower the frequency, the faster the convergence. With higher frequency, preprocessing (CCN) results in a slower convergence compared to PCC and CCG.

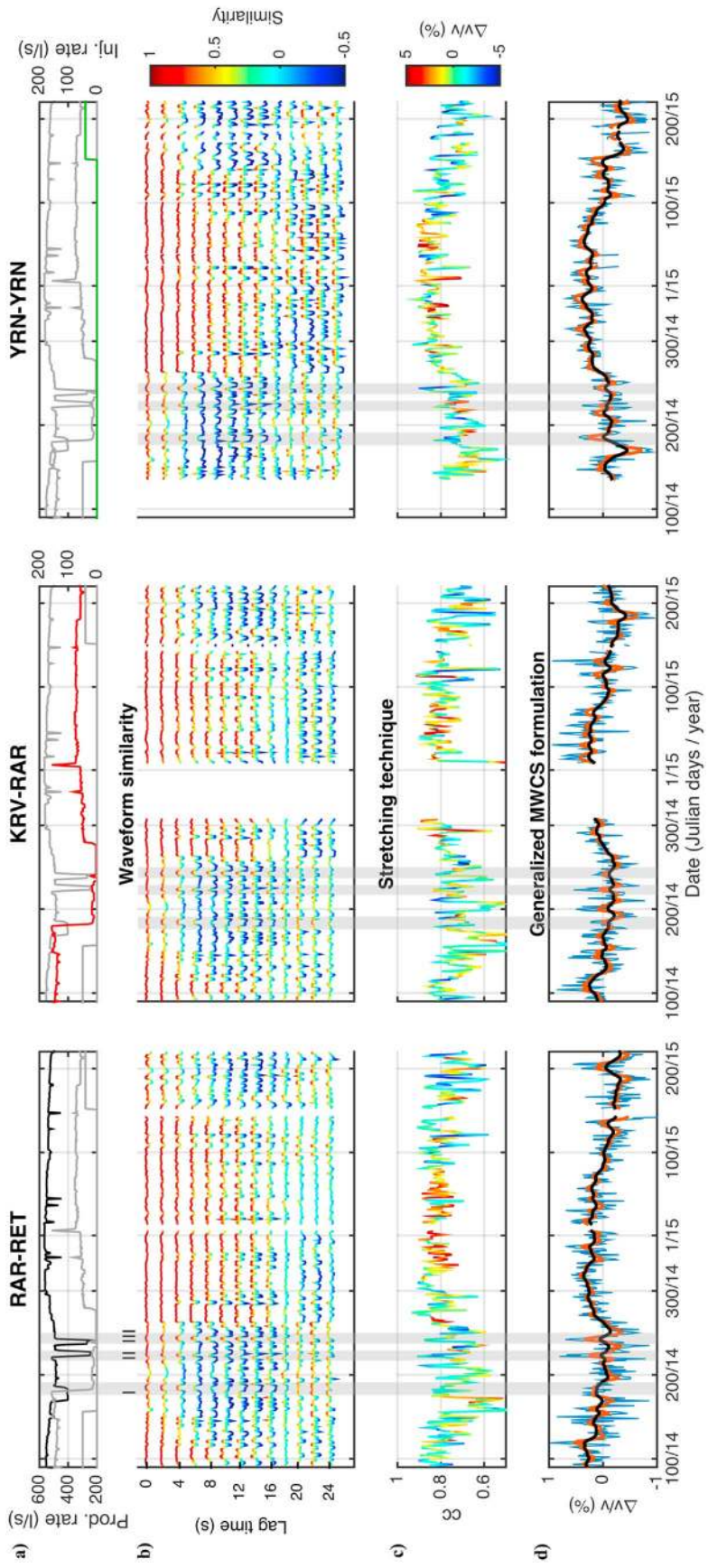

Figure 2. Results of the three different methodologies employed for the frequency band (0.1–1 Hz) for three station couples: RAR-RET (crossing the production area), KRV-RAR (crossing RN-20B well), and the autocorrelation of YRN (close to RN-34). (a) Production and injection rates of Reykjanes Geothermal System are represented in gray highlighting the closest well rate following the colors of Figure 1, and the production rate, in black. (b) Averaged waveform similarity values for negative and positive lag time windows of 6-s length. (c) Correlation coefficients obtained from the stretching technique; the color scale represents the computed velocity change. (d) Velocity changes computed by MWCS technique for three correlation lengths, $\beta = 5$ (blue), 10^3 (orange), and 10^4 (black). Gray shading indicates the three fluctuations of interest (I, II, and III).

Therefore, we primarily focus on the frequency band 0.1–1.0 Hz and stack correlations from 72 hr of seismic recordings for a stable convergence. The method employed will be PCC, because it is more sensitive to waveform changes (Schimmel et al., 1999) and the convergence of the three methods is similar for this frequency band (Figure S2).

3.3. Determination of Time-Lapse Changes

With ongoing production over a large area and various injection wells in the RGS, it is challenging to identify time-lapse changes in the coda associated with well operations. To ensure that our results are unbiased by the choice of the reference function, we use all three methods that are currently discussed in the literature to detect time-lapse changes: time evolution of waveform similarity (e.g.,D'Hour et al., 2015 ; SÁnchez-Pastor et al., 2018), stretching method (e.g., Brenguier et al., 2011; Hadziioannou et al., 2011; Obermann et al., 2014), and a generalized formulation of the moving window cross-spectral (MWCS) (Brenguier et al., 2014; Gómez-García et al., 2018). The first two methods require a noise response reference of the medium to quantify changes, which is calculated by stacking days with the highest production rate (excluding the days 210–300/2014).

We selected three station couples to study coda time-lapse changes detected with the above-mentioned methods (Figure 2): RAR-RET that crosses the production area, KRV-RAR crossing the injection well RN-20B, and YRN, which is the closest station to the tracer test well RN-34.

3.3.1. Waveform Similarity

Changes in waveform similarity may be due to structural changes in the medium due to variations of scattering properties (e.g., altered seismic discontinuities and fracturing). To detect such distortions, we compute the waveform similarity (D'Hour et al., 2015; SÁnchez-Pastor et al., 2018) between the reference and daily responses in various lag time windows of 6-s length (Figure 2b). The most prominent feature is a sinusoidal variation, which finds its maximum in January and minimum in mid-July and appears between 4 and 16 s of lag time. The production rate also follows this low-frequency variation (Figure 2a, black line).

Besides this long-term feature, we observe short-term fluctuations that are consistent over a broad range of lag times. While many of these fluctuations cannot be related to RGS activity, climatological data or seismicity, we highlight three similarity changes (Figure 2b, gray-shadowed rectangles and labeled I, II, and III), which are accompanying the largest changes in production/injection. The changes can be seen up to 6, 8, and 14 s of lag time in the three station couples.

3.3.2. Waveform Stretching

Mechanical changes in the medium typically produce a time shift in the later-arriving waves, when compared with a reference (e.g., Brenguier et al., 2011; Hadziioannou et al., 2009; Obermann et al., 2014). In Figure 2c, we show the velocity variation results averaged between 10 and 50 s of lag time. The evolution of the correlation coefficient also shows the large sinusoidal trend commented on in the previous section. We can also observe the local perturbations (I, II, and III) in all three station couples, although less clearly than from the waveform similarity analysis.

The correlation coefficient is around 0.8, and the observed velocity fluctuations are quite large. The stretching technique requires high coherence between reference and daily traces, which is not achieved in this study due to the strong variability of the seismic medium response. This coherence can be increased stacking more days for comparison and/or using a larger time shift in the coda. However, as we expect tiny changes that happen only over short periods of time, we prefer to keep our choice of parameters and remain aware of the ambiguity in the absolute values of the velocity variations.

3.3.3. Generalized MWCS Formulation

The MWCS technique quantifies the velocity variation of the medium by a linear adjustment of the time shift using several consecutive lag time windows in the frequency domain (Clarke et al., 2011). This approach assumes a homogenously distributed velocity change, contrary to classical stretching that allows to determine the lag time-dependent effect of localized changes (Obermann, Planès, Larose, & Campillo, 2013; Obermann et al., 2016, 2018).

Brenguier et al. (2014) generalized the MWCS technique to be independent of a reference function. The changes are retrieved comparing the velocity estimates from MWCS between all possible combinations of days. The characteristic correlation length (β) controls the distance between days to be correlated. Thus,

we can obtain long and short time variations of the velocity change time series. We employ this method for $\beta = 5$, 10^3, and 10^4, and the results obtained are shown in Figure 2d. As with the previous methods, the low-frequency sinusoidal tendency is clearly visible in all station couples. Moreover, a gradual negative trend is observed in the velocity variations. The small perturbations are more complicated to distinguish from others although the decrease in injection rate (I) is observed in KRV-RAR and YRN-YRN, the production volume change II in RAR-RET and KRV-RAR, and change III can be seen in all three couples. The uncertainties of the velocity change estimates for $\beta = 5$ are around 0.05%, which are small in comparison to the velocity changes analyzed.

4. Discussion

4.1. Time-Frequency Analysis

The time evolution of the waveform similarity and of velocity variations gives us an idea of the influence of the operations at the RGS on the surrounding area. Due to the lack of records prior to the well operations and also the complexity of the system, such time evolutions (in particular the seismic velocity variations) contain various fluctuations that are difficult to relate directly to natural or artificial processes.

In the following, we focus on the largest rate variations of the power plant (I, II, and III) and see if we can work out the time lag changes more clearly by decomposing the similarity curves in the time-frequency domain through the S transform (Stockwell et al., 1996)

$$S(\tau,f) = \int_{-\infty}^{+\infty} s(t) w(\tau - t, f) e^{i2\pi f t} \mathrm{d}t, \tag{1}$$

where $s(t)$ is the waveform similarity curve at a specific lag time window and $w(\tau - t,f)$ is a Gaussian function centered at time τ and width proportional to $1/f$. The S transform is based on the Fourier theory and related to the wavelet transform through a matrix multiplication (Schimmel et al., 2011; Ventosa et al., 2008).

We perform the S transform for the 1.5 years for all station couples, splitting them into two groups (crossing and not crossing the production area) to differentiate and analyze the observed waveform changes (Figure 3). Considering that the sample rate of the similarity time series is 1 day, the Nyquist frequency corresponds to 0.5 days^{-1}. On the other hand, the resolution at low frequencies is expected to be poor since the records are only 1.5 years long. The three changes in similarity are more prominent for the station couples that cross the production area. On the contrary, for stations outside this area, the similarity changes are smaller and show more variability (Figure 3b). In Figure 3c, such fluctuations emerge around 0.5 days^{-1}. Below $6{\cdot}10^{-3}$ days^{-1}, we can observe the long seasonal variation that we discussed in section 3.3 in both station groups, although it is more intense for the couples closer to the production area.

4.2. Spatial Distribution of the Changes

Comparing the results between the two station groups of Figure 3, we expect the biggest structural changes within the production area. For verification and further details, we also compute the spatial distribution of the scattering cross sections associated with the structural changes (I, II, III, and seasonal) based on probabilistic sensitivity kernels (e.g., Larose et al., 2010; Obermann, Planès, Larose, Sens-Schönfelder, & Campillo, 2013; Pacheco & Snieder, 2005). We assume surface waves dominance and use the solution of the 2-D radiative transfer equation to build sensitivity kernels (Paasschens, 1997; Sato, 1993; Shang & Gao, 1988) and a scattering mean free path of 30 km. These sensitivity kernels (K), the observed similarity changes (DC), and their scattering cross sections (σ) are related according to the following formula:

$$DC = \frac{c\sigma}{2} K, \tag{2}$$

where c is the effective wave speed that we fix at 3 km/s. We obtain the scattering cross sections from equation (2) by using the minimum square inversion method for linear problems (Tarantola & Valette, 1982). Since the three similarity peaks are in the seasonal variation minimum, the decorrelation is quantified as the similarity amplitude of such days whereas the seasonal change is computed as the difference between the averaged similarity in summer and winter.

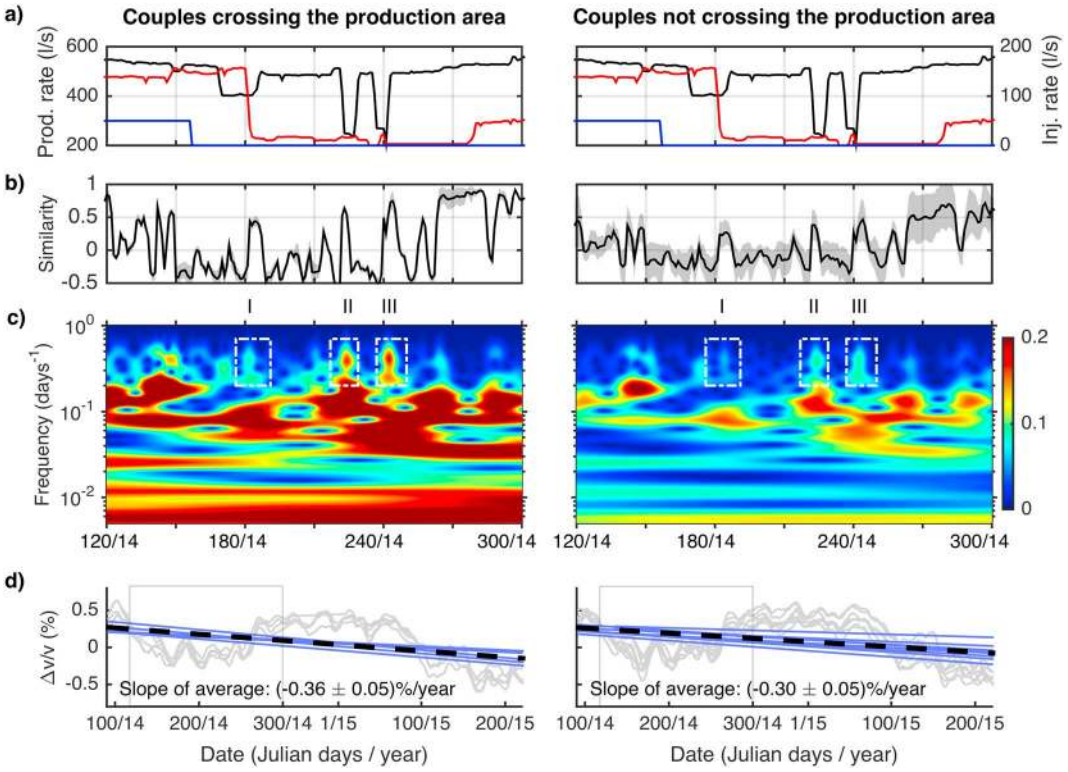

Figure 3. (a) Production and injection rate of Reykjanes Geothermal System. The colors are the same as on Figure 2a. (b) Average of similarity values of station couples that cross (left) and do not cross (right) the production area at 6-s lag time. Standard deviation is shown as gray shading. (c) Time-frequency amplitude spectra of the above similarity curves. The white boxes highlight the fluctuations I, II, and III. (d) Velocity variations measured using the generalized MWCS formulation for $\beta = 10^4$ (gray lines) of autocorrelations for the 1.5 years of study. The blue lines represent their linear regressions of every curve, and the dashed black line, the linear regression of the velocity variation average of the station group. The gray box marks the period of time of the upper panels.

Figure 4 shows the inversion results for the four similarity changes under study. Consistently, the larger the similarity change, the larger the observed scattering cross section. All structural changes, including the seasonal changes, are located around the production area and vanish with distance. In general, the values are smaller than in other studies, where volcanic eruption volumes (Obermann, Planès, Larose, Sens-

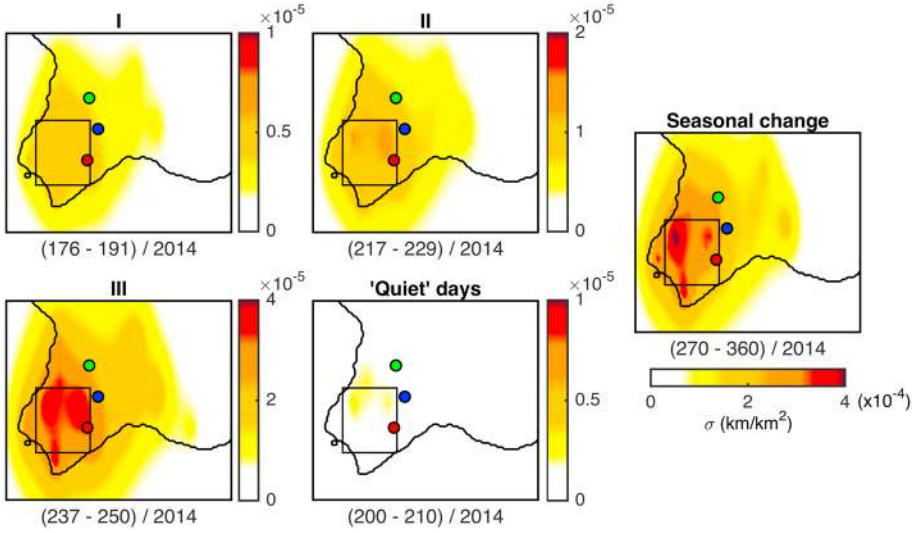

Figure 4. Scattering cross-section density maps at 6-s lag time for (a–c) the three highlighted periods in Figure 3 (I, II, and III), (d) an example of calmest days, and (e) the seasonal change.

Schönfelder, & Campillo, 2013; SÁnchez-Pastor et al., 2018) or 10^5 L of injection were studied (Hillers et al., 2015). For comparison, we compute the inversion during the "calmest" days 200–210 (2014), when the production rate remains constant with fluid injection almost 0 (Figure 4d).

4.3. Short- and Long-Term Effects of RGS

The short-term subsurface effects of the exploitation of the RGS are associated with sharp variations of water injection volume and energy production. These rapid fluctuations change the state of stress abruptly and distort wave propagation, which can be observed by SI. In the Reykjanes peninsula for frequencies of 0.1–1 Hz, the seismic velocity of surface waves is roughly 1.2 km/s (Jousset et al., 2016). The probed depth should therefore range between 0.5 and 12 km. The similarity change I, which is related to the largest injection-rate drop of RN-20B, appears at earlier lag times than the others. The associated structural changes are therefore shallower than those caused by production rate drops, which affect likely a deeper and wider zone of the surrounding medium. The changes are expected to be constrained to the first few kilometers of the crust. This corresponds to the approximate depth of water injection into the rock mass.

In monitoring studies with long seismic records, seasonal variations are typically observed (e.g., Gómez-García et al., 2018; Sens-Schönfelder & Wegler, 2006) and typically related to seasonal variations of the ocean noise directivity (Juretzek & Hadziioannou, 2016; Stutzmann et al., 2009), which affect the ballistic waves of the cross correlations (e.g., Froment et al., 2010; Hadziioannou et al., 2011). However, the effects of the seasonal variations are expected to be mostly homogeneous since the study area is very small. Nevertheless, we observe a more intense seasonal variation near the power plant (Figures 3c and 4e). The production rate varies depending on the power demand of the Icelandic population, and that is highest in winter and decreases during summer (Figure 3a). Indeed, the Pearson coefficient between the similarity curve at 6-s lag time and the smoothed production rate (without the abrupt changes) is estimated as 0.84 (supporting information Figure S3). Looking at days 120 (2014), 264 (2014), and 155 (2015), the similarity values suffer a sign switch too abrupt to come from a noise source distribution change and do not coincide with any production rate drop (Figures 2a and 2b). We are however inclined to believe that the production rate variations directly influence the subsurface and may be therefore in phase and overlap the variation due to changing noise sources (Figure 2). A possible interpretation is that the medium exhibits a production rate threshold, here estimated at about 520 L/s (Figure 2a). Once the production volume passes this tolerance threshold, the elastic properties of the medium change significantly. This threshold could be related to the permeability of the rock mass, which depends exponentially on the exposition time to hot water flows (Summers et al., 1978) and affects the pore pressure of the rocks (David et al., 1994).

Another long-term effect in the Reykjanes reservoir is the negative trend of the velocity variation time series (Figure 2d). As autocorrelations are more sensitive to local changes in the subsurface and probe larger depths (e.g., D'Hour et al., 2015; SÁnchez-Pastor et al., 2018), we compute linear regressions of the velocity variations from the generalized MWCS formulation of all autocorrelations within and outside the production area (Figure 3d). All autocorrelations show this particular velocity decrease being slightly stronger for the station couples that cross the production area. The slope of the velocity variation average represents a regional velocity decrease rate of 0.36%/year in the production area and 0.3%/year outside. Since the water volume injected is less than the extracted volume (Figure 2a), there is a water loss that is partially compensated by natural recharge into the system (Keiding et al., 2010). However, the consequent long-term decrease in pore pressure causes a contraction of the rock matrix and man-made subsidence of the peninsula (Keiding et al., 2010). This subsidence carries a density increase of rocks yielding the observed velocity decrease. The water deficit can play a further role in the observed seismic velocity, which decreases in high-porosity pyroclastic rocks as a function of water content (e.g., Kahraman et al., 2017). Note that the system seems to respond differently for short and long timescales; whereas the velocity variations increase for abrupt decreases in water extraction, those variations decrease over a timescale of years due to the water deficit. However, here we did not further analyze the physical processes that cause this different behavior.

5. Conclusions

The time evolution pattern of similarity and velocity changes has a rich frequency content that points to different timescale effects in the Reykjanes reservoir. We decompose the similarity time series into the time-frequency domain through the S transform, allowing us to clearly discriminate three fluctuations

associated to injection and production rate drops. The lack of seismic records during a calm period causes a strong variability of noise response reference of the medium. In these conditions, the reference unbiased MWCS analysis shows a great advantage compared to the classical stretching method. There are many fluctuations in the time series that do not match with the timing of water injection and production volume variations and could be caused by conduit collapses, water saturation, or diverse instabilities in the medium. In the long term, the power plant subsurface shows a seasonal variation that might be associated with the energy demand. Furthermore, the increasing water deficit of this hydrothermal system produces a slow velocity decrease of 0.36%/year in the surrounding medium.

Acknowledgments
We warmly thank Ómar Sigurðsson from HS Orka (the owner of Reykjanes Geothermal plant) for providing us with the production and injection rate data (https://www.hsorka.is). In addition, we would like to thank Hanna Blanck, Kristján Ágústsson, and Gylfi Páll Hersir, all from Iceland GeoSurvey (ÍSOR, http://en.isor.is/), for their help and for providing the data of the stations with the short-period Lennartz sensors (operated on behalf of HS Orka). The climatological data can be requested from https://en.vedur.is/. The research efforts by C. W. has received funding from the European Community's Seventh Framework Programme under grant agreement 608553 (Project IMAGE, http://www.image-fp7.eu). Pilar Sánchez-Pastor acknowledges funding from the Spanish Ministry of Economy and Competitiveness (project MISTERIOS, CGL2013-48601-C2-1-R). We also thank Editor Rebecca Carey and the two reviewers Gerrit Olivier and Clare Donaldson for comments that helped improve the manuscript.

References

Aki, K. (1957). Space and time spectra of stationary stochastic waves, with special reference to microtremors. *Bulletin of the Earthquake Research Institute*, *35*, 415–457. http://hdl.handle.net/2261/11892

Axelsson, G., Arnaldsson, A., Berthet, J.-c. C., Bromley, C. J., Gudnason, E. Á., Hreinsdóttir, S., et al. (2015). Renewability assessment of the Reykjanes Geothermal System, SW-Iceland. In Proceedings World Geothermal Congress, 10.

Bakulin, A., & Calvert, R. (2006). The virtual source method: Theory and case study. *Geophysics*, *71*(4), SI139–SI150. https://doi.org/10.1190/1.2216190

Bensen, G. D., Ritzwoller, M. H., Barmin, M. P., Levshin, A. L., Lin, F., Moschetti, M. P., et al. (2007). Processing seismic ambient noise data to obtain reliable broad-band surface wave dispersion measurements. *Geophysical Journal International*, *169*(3), 1239–1260. https://doi.org/10.1111/j.1365-246X.2007.03374.x

Beroza, G. C., Cole, A. T., & Ellsworth, W. L. (1995). Stability of coda wave attenuation during the Loma Prieta, California, earthquake sequence. *Journal of Geophysical Research*, *100*(B3), 3977–3987. https://doi.org/10.1029/94JB02574

Blanck H., Jousset P., Agustsson, G.P. Hersir, G. P. & Flovenz, O. G. (2016). Analysis of seismological data on Reykjanes peninsula, Iceland. Extended abstract of the European Geothermal Congress, Strasbourg France.

Brenguier, F., Campillo, M., Takeda, T., Aoki, Y., Shapiro, N. M., Briand, X., et al. (2014). Mapping pressurized volcanic fluids from induced crustal seismic velocity drops. *Science*, *345*(6192), 80–82. https://doi.org/10.1126/science.1254073

Brenguier, F., Clarke, D., Aoki, Y., Shapiro, N. M., Campillo, M., & Ferrazzini, V. (2011). Monitoring volcanoes using seismic noise correlations. *Comptes Rendus Geoscience*, *343*(8-9), 633–638. https://doi.org/10.1016/j.crte.2010.12.010

Claerbout, J. (1968). Synthesis of a layered medium from its acoustic transmission response. *Geophysics*, *33*(2), 264–269. https://doi.org/10.1190/1.1439927

Clarke, D., Zaccarelli, L., Shapiro, N. M., & Brenguier, F. (2011). Assessment of resolution and accuracy of the Moving Window Cross Spectral technique for monitoring crustal temporal variations using ambient seismic noise. *Geophysical Journal International*, *186*(2), 867–882. https://doi.org/10.1111/j.1365-246X.2011.05074.x

David, C., Wong, T. F., Zhu, W., & Zhang, J. (1994). Laboratory measurement of compaction-induced permeability change in porous rocks: Implications for the generation and maintenance of pore pressure excess in the crust. *Pure and Applied Geophysics*, *143*(1-3), 425–456. https://doi.org/10.1007/BF00874337

D'Hour, V., Schimmel, M., Do Nascimento, A. F., Ferreira, J. M., & Lima Neto, H. C. (2015). Detection of subtle hydromechanical medium changes caused by a small-magnitude earthquake swarm in NE Brazil. *Pure and Applied Geophysics*, *173*(4), 1097–1113. https://doi.org/10.1007/s00024-015-1156-0

Draganov, D., Wapenaar, K., Mulder, W., Singer, J., & Verdel, A. (2007). Retrieval of reflections from seismic background-noise measurements. *Geophysical Research Letters*, *34*, L04305. https://doi.org/10.1029/2006GL028735

Duvall, T. L., Jefferies, S. M., Harvey, J. W., & Pomerantz, M. A. (1993). Time-distance helioseismology. *Nature*, *362*(6419), 430–432. https://doi.org/10.1038/362430a0

Flóvenz, Ó. G., Ágústsson, K., Guðnason, E. A., & KristjÁnsdóttir, S. (2015). Reinjection and induced seismicity in geothermal fields in Iceland. Proceedings World Geothermal Congress 2015, Melbourne, Australia

Fricke, J. T., Evers, L. G., Smets, P. S. M., Wapenaar, K., & Simons, D. G. (2014). Infrasonic interferometry applied to microbaroms observed at the Large Aperture Infrasound Array in the Netherlands. *Journal of Geophysical Research: Atmospheres*, *119*, 9654–9665. https://doi.org/10.1002/2014JD021663

Froment, B., Campillo, M., Roux, P., Gouédard, P., Verdel, A., & Weaver, R. (2010). Estimation of the effect of non-isotropic distributed energy on the apparent arrival time in correlations. *Geophysics*, *75*(5), SA85–SA93. https://doi.org/10.1190/1.3483102

Gómez-García, C., Brenguier, F., Boué, P., Shapiro, N. M., Droznin, D. V., Droznina, S. Y., et al. (2018). Retrieving robust noise-based seismic velocity changes from sparse data sets: Synthetic tests and application to Klyuchevskoy volcanic group (Kamchatka). *Geophysical Journal International*, *214*(2), 1218–1236.

Gudmundsson, A. (1995). Ocean-ridge discontinuities in Iceland. *Journal of the Geological Society*, *152*(6), 1011–1015. https://doi.org/10.1144/GSL.JGS.1995.152.01.22

Gudmundsson, J., & Thórhallsson, S. (1986). The Svartsengi Reservoir in Iceland. *Geothermics*, *15*(1), 3–15. https://doi.org/10.1016/0375-6505(86)90025-8

Hadziioannou, C., Larose, E., Baig, A., Roux, P., & Campillo, M. (2011). Improving temporal resolution in ambient noise monitoring of seismic wave speed. *Journal of Geophysical Research*, *116*, B07304. https://doi.org/10.1029/2011JB008200

Hadziioannou, C., Larose, E., Coutant, O., Roux, P., & Campillo, M. (2009). Stability of monitoring weak changes in multiply scattering media with ambient noise correlation: Laboratory experiments. *The Journal of the Acoustical Society of America*, *125*(6), 3688–3695. https://doi.org/10.1121/1.3125345

Haney, M. M. (2009). Infrasonic ambient noise interferometry from correlations of microbaroms. *Geophysical Research Letters*, *36*, L19808. https://doi.org/10.1029/2009GL040179

Hillers, G., Husen, S., Obermann, A., Planès, T., Larose, E., & Campillo, M. (2015). Noise-based monitoring and imaging of aseismic transient deformation induced by the 2006 Basel reservoir stimulation. *Geophysics*, *80*(4), KS51–KS68. https://doi.org/10.1190/geo2014-0455.1

Hirschberg, S., Wiemer, S. & Burgherr, P. (2015). Energy from the Earth, in deep geothermal as a resource for the future?, edited by S. Hirschberg, S. Wiemer, and P. Burgherr, vdf Hochschulverlag, Zürich., https://doi.org/10.3218/3655-8.

International Energy Agency (IEA). Medium-term renewable energy market report 2018. Technical report, Paris (2018).
Jousset, P., Blanck, H., Franke, S., Metz, M., Ágústsson, K., Verdel, A., et al. (2016). Seismic tomography in Reykjanes, SW Iceland. Paper presented at European Geothermal Congress 2016, Strasbourg, France.
Juretzek, C., & Hadziioannou, C. (2016). Where do ocean microseisms come from? A study of Love-to-Rayleigh wave ratios. *Journal of Geophysical Research: Solid Earth*, *121*, 6741–6756. https://doi.org/10.1002/2016JB013017
Kahraman, S., Fener, M., & Kilic, C. O. (2017). Estimating the wet-rock P-wave velocity from the dry-rock P-wave velocity for pyroclastic rocks. *Pure and Applied Geophysics*, *174*(7), 2621–2629. https://doi.org/10.1007/s00024-017-1561-7
Keiding, M., Arnadóttir, T., Jónsson, S., Decriem, J., & Hooper, A. (2010). Plate boundary deformation and man-made subsidence around geothermal fields on the Reykjanes Peninsula, Iceland. *Journal of Volcanology and Geothermal Research*, *194*(4), 139–149. https://doi.org/10.1016/j.jvolgeores.2010.04.011
Kohler, M. D., Heaton, T. H., & Bradford, S. C. (2007). Propagating waves in the steel, moment-frame factor building recorded during earthquakes. *Bulletin of the Seismological Society of America*, *97*(4), 1334–1345. https://doi.org/10.1785/0120060148
Larose, E., Planes, T., Rossetto, V., & Margerin, L. (2010). Locating a small change in a multiple scattering environment. *Applied Physics Letters*, *96*(20). https://doi.org/10.1063/1.3431269
Lehujeur, M., Vergne, J., Schmittbuhl, J., & Maggi, A. (2015). Characterization of ambient seismic noise near a deep geothermal reservoir and implications for interferometric methods: A case study in northern Alsace, France. *Geothermal Energy*, *3*(1). https://doi.org/10.1186/s40517-014-0020-2
Obermann, A., Froment, B., Campillo, M., Larose, E., Planès, T., Valette, B., et al. (2014). Seismic noise correlations to image structural and mechanical changes associated with the Mw7.9 2008 Wenchuan earthquake. *Journal of Geophysical Research: Solid Earth*, *119*, 3155–3168. https://doi.org/10.1002/2013JB010932
Obermann, A., Kraft, T., Larose, E., & Wiemer, S. (2015). Potential of ambient seismic noise techniques to monitor the St. Gallen geothermal site (Switzerland). *Journal of Geophysical Research: Solid Earth*, *120*, 4301–4316. https://doi.org/10.1002/2014JB011817
Obermann, A., Planès, T., Hadziioannou, C., & Campillo, M. (2016). Lapse-time-dependent coda-wave depth sensitivity to local velocity perturbations in 3-D heterogeneous elastic media. *Geophysical Journal International*, *207*(1), 59–66. https://doi.org/10.1093/gji/ggw264
Obermann, A., Planès, T., Larose, E., & Campillo, M. (2013). Imaging preeruptive and coeruptive structural and mechanical changes of a volcano with ambient seismic noise. *Journal of Geophysical Research: Solid Earth*, *118*, 6285–6294. https://doi.org/10.1002/2013JB010399
Obermann, A., Planès, T., Larose, E., & Campillo, M. (2018). 4-D imaging of subsurface changes with coda waves: Numerical studies of 3-D combined sensitivity kernels and applications to the Mw 7.9, 2008 Wenchuan Earthquake. *Pure and Applied Geophysics*, *176*(3), 1243–1254. https://doi.org/10.1007/s00024-018-2014-7
Obermann, A., Planès, T., Larose, E., Sens-Schönfelder, C., & Campillo, M. (2013). Depth sensitivity of seismic coda waves to velocity perturbations in an elastic heterogeneous medium. *Geophysical Journal International*, *194*(1), 372–382. https://doi.org/10.1093/gji/ggt043
Paasschens, J. C. J. (1997). Solution of the time-dependent Boltzmann equation. *Physical Review E*, *56*(1), 1135–1141. https://doi.org/10.1103/PhysRevE.56.1135
Pacheco, C., & Snieder, R. (2005). Time-lapse travel time change of multiply scattered acoustic waves. *The Journal of the Acoustical Society of America*, *118*(3), 1300–1310. https://doi.org/10.1121/1.2000827
Poupinet, G., Ellsworth, W. L., & Frechet, J. (1984). Monitoring velocity variations in the crust using earthquake doublets: An application to the Calaveras fault, California. *Journal of Geophysical Research*, *89*(B7), 5719–5731. https://doi.org/10.1029/JB089iB07p05719
Ragnarsson, Á. (2013). Geothermal energy use, country update for Iceland. Paper presented at European Geothermal Congress 2013, Pisa, Italy, 11.
Romero, P., & Schimmel, M. (2018). Mapping the basement of the Ebro Basin in Spain with seismic ambient noise autocorrelations. *Journal of Geophysical Research: Solid Earth*, *123*, 5052–5067. https://doi.org/10.1029/2018JB015498
Roux, P., & Fink, M. (2003). Green's function estimation using secondary sources in a shallow water environment. *The Journal of the Acoustical Society of America*, *113*(3), 1406–1416. https://doi.org/10.1121/1.1542645
Roux, P., Sabra, K. G., Gerstoft, P., Kuperman, W. A., & Fehler, M. C. (2005). P-waves from cross-correlation of seismic noise. *Geophysical Research Letters*, *32*, L19303. https://doi.org/10.1029/2005GL023803
SÁnchez-Pastor, P., Obermann, A., & Schimmel, M. (2018). Detecting and locating precursory signals during the 2011 El Hierro, Canary Islands, submarine eruption. *Geophysical Research Letters*, *45*, 10,288–10,297. https://doi.org/10.1029/2018GL079550
Sato, H. (1993). Energy transportation in one- and two-dimensional scattering media-analytic solutions of the multiple isotropic scattering model. *Geophysical Journal International*, *112*(1), 141–146. https://doi.org/10.1111/j.1365-246X.1993.tb01443.x
Schimmel, M. (1999). Phase cross correlations: Design, comparisons, and applications. *Bulletin of the Seismological Society of America*, *89*(5), 1366–1378.
Schimmel, M., Stutzmann, E., & Gallart, J. (2011). Using instantaneous phase coherence for signal extraction from ambient noise data at a local to a global scale. *Geophysical Journal International*, *184*(1), 494–506. https://doi.org/10.1111/j.1365-246X.2010.04861.x
Schimmel, M., Stutzmann, E., & Ventosa, S. (2018). Low-frequency ambient noise autocorrelations: Waveforms and normal modes. *Seismological Research Letters*, *89*(4), 1488–1496. https://doi.org/10.1785/0220180027
Sens-Schönfelder, C., & Wegler, U. (2006). Passive image interferometry and seasonal variations of seismic velocities at Merapi Volcano, Indonesia. *Geophysical Research Letters*, *33*, L21302. https://doi.org/10.1029/2006GL027797
Sens-Schönfelder, C., & Wegler, U. (2011). Passive image interferometry for monitoring crustal changes with ambient seismic noise, C. R. *Geosciences*, *343*(8-9), 639–651. https://doi.org/10.1016/j.crte.2011.02.005
Shang, T., & Gao, L. (1988). Transportation theory of multiple scattering and its application to seismic coda waves of impulsive source. *Scientia Sinica*, *31*, 1503–1514.
Shapiro, N., Campillo, M., Stehly, L., & Ritzwoller, M. (2005). High-resolution surface-wave tomography from ambient seismic noise. *Science (New York, N.Y.)*, *307*(5715), 1615–1618. https://doi.org/10.1126/science.1108339
Snieder, R., Grêt, A., Douma, H., & Scales, J. (2002). Coda wave interferometry for estimating nonlinear behaviour in seismic velocity. *Science*, *295*(5563), 2253–2255. https://doi.org/10.1126/science.1070015
Snieder, R., & Safak, E. (2006). Extracting the building response using seismic interferometry: Theory and application to the Millikan Library in Pasadena, California. *Bulletin of the Seismological Society of America*, *96*(2), 586–598. https://doi.org/10.1785/0120050109
Stähler, S. C., Sens-Schönfelder, C., & Niederleithinger, E. (2011). Monitoring stress changes in a concrete bridge with coda wave interferometry. *The Journal of the Acoustical Society of America*, *129*(4), 1945–1952. https://doi.org/10.1121/1.3553226

Stockwell, R. G., Mansinha, L., & Lowe, R. P. (1996). Localization of the complex spectrum: The S transform. *IEEE Transactions on Signal Processing*, *44*(4), 998–1001. https://doi.org/10.1109/78.492555

Stutzmann, E., Schimmel, M., Patau, G., & Maggi, A. (2009). Global climate imprint on seismic noise. *Geochemistry, Geophysics, Geosystems*, *10*, Q11004. https://doi.org/10.1029/2009GC002619

Summers, R., Winkler, K., & Byerlee, J. (1978). Permeability changes during the flow of water through Westerly Granite at temperatures of 100–400 C. *Journal of Geophysical Research*, *83*(B1), 339–344. https://doi.org/10.1029/JB083iB01p00339

Tarantola, A., & Valette, B. (1982). Generalized non-linear inverse problems solved using the least-squares criterion. *Reviews of Geophysics*, *20*(2), 219–232. https://doi.org/10.1029/RG020i002p00219

Tsai, V. C. (2009). On establishing the accuracy of noise tomography traveltime measurements in a realistic medium. *Geophysical Journal International*, *178*(3), 1555–1564. https://doi.org/10.1111/j.1365-246X.2009.04239.x

Ventosa, S., Simon, C., Schimmel, M., Dañobeitia, J. J., & Manuel, A. (2008). S-transform from a wavelets point of view. *IEEE Transactions on Signal Processing*, *56*(7), 2771–2780. https://doi.org/10.1109/TSP.2008.917029

Weaver, R., Froment, B., & Campillo, M. (2009). On the correlation of non-isotropically distributed ballistic scalar diffuse waves. *The Journal of the Acoustical Society of America*, *126*(4), 1817–1826. https://doi.org/10.1121/1.3203359

Weemstra, C., Obermann, A., Verdel, A., Paap, B., Blanck, H., Guðnason, E. Á., et al. (2016). Time-lapse seismic imaging of the Reykjanes geothermal reservoir. *Paper presented at Proceedings European Geothermal Congress 2016, Strasbourg, France*.

Woolfe, K. F., Lani, S., Sabra, K. G., & Kuperman, W. (2015). Monitoring deep-ocean temperatures using acoustic ambient noise. *Geophysical Research Letters*, *42*, 2878–2884. https://doi.org/10.1002/2015GL063438